Flow Turbulence Combust (2016) 97:609–629
DOI 10.1007/s10494-015-9702-5

Effects of Spray and Turbulence Modelling on the Mixing and Combustion Characteristics of an *n*-heptane Spray Flame Simulated with Dynamic Adaptive Chemistry

Zhen Lu[1] · Lei Zhou[1,2] · Zhuyin Ren[1,3] · Tianfeng Lu[4] · Chung K. Law[1,5]

Received: 19 May 2015 / Accepted: 30 December 2015 / Published online: 13 January 2016

Abstract Accurate modelling of spray combustion process is essential for efficiency improvement and emissions reduction in practical combustion engines. In this work, both unsteady Reynolds-averaged Navier-Stokes (URANS) simulations and large eddy simulations (LES) are performed to investigate the effects of spray and turbulence modelling on the mixing and combustion characteristics of an *n*-heptane spray flame in a constant volume chamber at realistic conditions. The non-reacting spray process is first simulated with URANS to investigate the effects of entrainment gas-jet model on the penetration characteristics and fuel vapor distributions. It is found that the droplet motion near the nozzle has significant influence on the fuel vapor distribution, while the liquid penetration length is controlled by the evaporation process and insensitive to gas-jet model. For the case considered, both URANS with the gas-jet model and large eddy simulations can properly predict the vapor penetration. For the combustion characteristics, it is found that LES yields better predictions in the global combustion characteristics. The URANS with gas jet model

✉ Zhuyin Ren
zhuyinren@mail.tsinghua.edu.cn

[1] Center for Combustion Energy, Tsinghua University, Beijing 100084, China

[2] State Key Laboratory of Engines, Tianjin University, Tianjin 300072, China

[3] School of Aerospace Engineering, Tsinghua University, Beijing, 100084, China

[4] Department of Mechanical Engineering, University of Connecticut, Storrs, CT 06269, USA

[5] Department of Mechanical and Aerospace Engineering, Princeton University, Princeton, NJ 08540, USA

yields a comparable flame length and lift-off-length (LOL) to LES, but results in a larger ignition delay time compared to the experimental data. Another focus of this work is to qualify the convergence characteristics of the dynamic adaptive chemistry (DAC) method in these transient combustion simulations, where DAC is applied to reduce the mechanism locally and on-the-fly to accelerate chemistry calculations. The instantaneous flame structures and global combustion characteristics such as ignition delay time, flame lift-off length and emissions are compared between simulations with and without DAC. For URANS, good agreements are observed both on instantaneous flame structures and global characteristics. For LES, it is shown that the errors incurred by DAC are small for scatter distributions in composition space and global combustion characteristics, while they may significantly affect instantaneous flame structures in physical space. The study reveals that for DAC application in transient simulations, global or statistic information should be used to assess the accuracy, such as manifolds in composition space, conditional quantities and global combustion characteristics. For the cases investigated, a speed-up factor of more than two is achieved by DAC with a 92-species skeletal mechanism with less than 0.2 % and 3.0 % discrepancy in ignition delay and LOL, respectively.

Keywords Gas jet model · Dynamic adaptive chemistry · Large-eddy simulations · Spray flame · Detailed chemical kinetics

1 Introduction

Accurate modelling of spray combustion process is essential for efficiency improvement and emissions reduction in diesel engines [1]. Multi-dimensional computational fluid dynamics of reactive flows has become an indispensable and effective tool for probing the multi-scale physicochemical processes involved in diesel spray combustion such as liquid breakups, mixing, ignition and emission formation, parts of which are difficult to access in experiments [2]. One widely employed approach for simulating spray combustion is the Lagrangian-droplet-and-Eulerian-fluid (LDEF) method [1], which describes the liquid phase by tracking discrete liquid droplets in the Lagrangian system and solve the gas phase as a continuum fluid in the Eulerian system.

In this work, URANS and LES simulations via LDEF with detailed chemistry are performed to simulate the well-documented *n*-heptane spray flame in a constant volume combustion chamber, often denoted as the "Spray H" [2], from the Sandia National Laboratories, with experimental data being available from the engine combustion network (ECN) [3]. A number of studies with detailed chemistry [4–13] have been reported to investigate the importance of the chemical kinetics and turbulence-chemistry interaction (TCI) on the flame stabilization and auto-ignition process in "Spray H". It is observed that, compared with the experimental data, the transported probability density function (PDF) simulations considering turbulence-chemistry interaction are more accurate than the well stirred reactor (WSR) model with TCI neglected [6]. Systematic studies of this flame using the URANS/transported PDF method [7] and URANS/WSR with reconstructed PDF of mixture fractions [14] imply that the importance of TCI rises at low initial ambient temperatures and low oxygen levels. Large eddy simulations of the "Spray H" have also been reported recently [4, 8, 9]. Som et al. [8] demonstrated the advantages of LES for predicting the

instantaneous behavior of the flame, while the predictions for the global parameters such as ignition delay time and quasi-steady LOL from URANS and LES are close.

Instead of investigating the importance of chemical kinetics and TCI on the flame stabilization and auto-ignition process in "Spray H", one focus of this study is to investigate the effects of spray and turbulence modelling on the mixing and combustion characteristics of the "Spray H" flame. For practical importance, fuel distribution, crucial to the ignition and emission characteristics, has to be determined accurately. Previous studies [15–18] found that RANS simulations with the LDEF method may lead to incorrect momentum coupling between gas-liquid-phases, resulting in mesh-dependent predictions of liquid penetration and fuel distribution. For example, Beard et al. [16, 17] found that the calculated relative velocity between the two phases is mesh-dependent, which may result in lower axial velocity and incorrect liquid and vapor penetration lengths. Currently the improved spray model based on gas-jet theory can effectively reduce the mesh dependence for spray evaporation process and improve the predictions of spray penetration [18], although in-depth analyses of the mixture fraction distribution and ignition are rarely reported. In this study URANS of the "Spray H" with/without gas jet model are firstly performed to investigate the penetration of liquid and vapor phases together with an analysis of fuel distribution compared to experimental data. Then large eddy simulations of the "Spray H", which directly resolve the large scale unsteady motions that account for the bulk spatial transportation and therefore can significantly improve the accuracy of penetration prediction, are performed with results compared with the RANS simulations to examine the impact of turbulence models on the mixing and ignition characteristics.

It is essential though challenging to incorporate detailed chemical kinetics into the spray combustion simulations for accurate prediction of ignition and emissions due to the large number of chemical species and wide range of chemical timescales involved [19, 20]. The set of nonlinear stiff ODEs governing chemical kinetics are large, leading to unaffordable computational expenses for multi-dimensional simulations. Of the frequently used chemistry acceleration approaches [21–28], dynamic adaptive chemistry (DAC), which has recently gained significant interests [29–34], is employed to accelerate the chemistry calculation in this study. It accelerates the time integration of the governing ODEs by reducing its size through the elimination of unimportant species and reactions. The on-the-fly reduction are achieved through directed relation graph (DRG) or other fast reduction methods [35–39]. DAC has been successfully demonstrated in multi-dimensional (unsteady) RANS simulations of turbulent combustion processes in internal combustion engines [32–34]. However there is no detailed study on the performance of DAC in LES simulations, though the application of DAC in LES is straightforward. Specifically the convergence characteristics of LES-DAC simulations with respect to the reduction threshold in instantaneous flame structures as well as global combustion characteristics have not been thoroughly investigated. Hence another focus of the study is to investigate the solution convergence characteristics in "Spray H" with DAC by examining the predictions of instantaneous flame structures and global combustion characteristics such as ignition delay time, flame lift-off length (LOL) and emissions.

The article is organized as follows. In Section 2, the computational models are presented, including the flow solver, a brief overview of gas jet theory and DAC, and the detailed simulation settings. The flow and combustion characteristics of Spray H from URANS and LES simulations are analysed in Section 3. The effect of DAC on instantaneous flame struc-

tures, manifolds in composition space and key combustion characteristics are presented in Section 4. Conclusions are in Section 5.

2 Computational Methods

2.1 Flow solver

The numerical scheme employed is based on the Arbitrary Lagrangian-Eulerian method with finite volume method [40]. For the continuum phase in URANS, a RNG $k-\varepsilon$ turbulence model [40] as the default model is employed with model parameters $C_\mu = 0.085$, $C_{\varepsilon 1} = 1.42$, $C_{\varepsilon 2} = 1.68$, $C_{\varepsilon s} = 1.50$, $\mathrm{Pr}_k = 1.39$, and $\mathrm{Pr}_\varepsilon = 1.396$. For comparison, simulations with the standard $k-\varepsilon$ turbulence model are also performed with model parameters $C_{\varepsilon 1} = 1.6$, $C_{\varepsilon 2} = 1.92$, $C_{\varepsilon 3} = -1.0$ $\mathrm{Pr}_k = 1.0$, and $\mathrm{Pr}_\varepsilon = 1.3$. For LES, a third-order Monotone Upstream-centered Schemes for Conservation Laws (MUSCL) [41] is implemented to obtain high order accuracy for the convection term. To describe the effects of the filtered small scale turbulence, a k-equation sub-grid turbulent kinetic energy model with $C_\mu = 0.067$ and $C_\varepsilon = 0.916$ [42] is implemented.

For the dispersed phase, the discrete droplet model [40] is applied, with the droplet particles tracked by solving the droplet velocity, mass, and temperature equations using the Lagrangian method. The primary and secondary liquid breakups are modelled by the Kelvin-Helmholtz and Rayleigh-Taylor model (KH-RT) [43]. In the KH-RT model, the model parameters B_0 and B_1, which are used to calculate the size of new droplet after breakup and the time scale of KH breakup, are set to be 0.61 and 18.0, respectively. The model parameters C_{RT} and C_τ are 0.1 and 0.5, respectively. The collision and coalescence model employed is that proposed by O'Rourke [44]. The interactions between the two phases are described through a two-way coupling, i.e. "gas-to-liquid" and "liquid-to-gas". In "gas-to-liquid", the changes of the droplet velocity in the computational domain are attributed to the drag force $F_{i,d}$ on droplet and calculated by the relative velocity between the droplet and the gas. In the "liquid-to-gas" aspect, the effects of liquid motion on the gas phase are treated as the Lagrangian source terms in the Eulerian momentum equation. Note that in LES the subgrid dispersion velocity model [45] is employed to calculate the effects of turbulent flows on droplets. Furthermore, the spray source term model [46] with a twice-test filtering subgrid gas velocity treatment is used to account for the spray effects on the subgrid turbulent kinetic energy.

To describe the gas-phase combustion, an n-heptane skeletal mechanism in conjunction of the well stirred reactor (WSR) model is employed in the simulations. The updated 92-species mechanism consists of 88-species, 387-reaction n-heptane mechanism [47] and a 13-step NO sub-mechanism [48]. Note that the employed 88-species n-heptane skeletal mechanism is reduced from the detailed 561-species LLNL mechanism [19, 20] by applying the DRG reduction over a wide range of thermo-chemical conditions to eliminate the unimportant species and reactions. Based on the previous findings [7, 14], the WSR model, though less accurate than transport PDF methods is sufficient for the purpose of investigating the fuel vapor penetration length and the solution convergence characteristics in URANS-DAC and LES-DAC simulations for the studied conditions.

2.2 Gas jet theory

The droplet particles are tracked by solving the equations for the droplet position, velocity, mass, and temperature,

$$\frac{dx_{d,i}}{dt} = v_{d,i} \tag{1}$$

$$\frac{dv_{d,i}}{dt} = \frac{F_{i,d}}{m_d} \tag{2}$$

$$\frac{dT_d}{dt} = \frac{1}{m_d C_{p,l}} \left(Q + \dot{m}_d l_v\right) \tag{3}$$

$$\frac{dm_d}{dt} = 4\pi\rho_l r_d^2 \frac{dr_d}{dt} \tag{4}$$

where $x_{d,i}$ and $v_{d,i}$ are the components of the droplet position and velocity respectively, T_d the droplet temperature, $m_d = 4/3\pi\rho_l r_d^3$ the droplet mass, $\mathrm{Q} = K_{air}\left(\hat{T}\right)(T - T_d)\mathrm{Nu}_d/2r_d$ the conductive heat flux through the droplet surface, T the ambient gas temperature, $\hat{T} = (T + 2T_d)/3$, Nu_d the droplet Nusselt number, $C_{p,l}$ the heat capacity of the liquid phase, and l_v the latent heat of vaporization. The drag on a liquid drop is modelled as:

$$\frac{F_{i,d}}{m_d} = \frac{3}{8}\frac{\rho}{\rho_l}\frac{V_{rel}}{r_d}\left(\tilde{u}_i - v_{d,i}\right) C_D \tag{5}$$

where $V_{rel} = \left|\tilde{u}_i + u'_{p,i} - v_{d,i}\right|$ is the magnitude of the relative velocity between the liquid droplet and the gas, $\tilde{u}_i$ the surrounding gas velocity, $u'_{p,i}$ the dispersion velocity, ρ_l the liquid droplet density, and r_d the radius. C_D is the drop drag coefficient given by

$$C_D = \begin{cases} \frac{24}{Re_d}\left(1 + 16Re_d^{23}\right) & Re_d < 1000 \\ 0.424 & Re_d > 1000 \end{cases} \tag{6}$$

Previous studies [49, 50] found that the predictions of vapor penetration depths and consequently the ignition characteristics from the LDEF method are mesh-dependent. The major reason is that the predicted relative velocity between droplets and gas is mesh-dependent. The gas-jet theory [49] can effectively reduce the grid-dependency through prescribing the axial component $\tilde{u}_z$ of the gas phase relative velocity V_{rel} in droplet equations. For the gas-jet model [51], it is given as

$$\tilde{u}_z = \min\left[U_{inj}, \frac{3U_{inj}^2 d_{eq}^2}{K_{entr} z}\left(\frac{1}{\left(1 + \frac{12r^2}{K_{entr}^2 z^2}\right)^2}\right)\right] \tag{7}$$

where K_{entr} is a model constant taken to be 0.45, as suggested by Abani et al. [51], U_{inj} the injection velocity of the liquid jet, which is assumed to be the injection velocity of the gas jet, z the axial distance of the droplet parcel from the nozzle and r the radial distance of the parcel form the spray axis. From the above equation, the relative velocity between the surrounding gas and droplets in the near-nozzle region is assumed to be around zero. The equivalent diameter d_{eq} is defined as: $d_{\mathrm{eq}} = d_{noz}\sqrt{\rho_l/\rho_g}$, where d_{noz} is the nozzle diameter, and ρ_g the densities of gas phase.

In the sub-grid one equation turbulent kinetic energy equation (k-equation model), the spray source term $\overline{\dot{W}^s}$ is simply defined as in [46], $\overline{\dot{W}^s} \equiv -F_i u_i'$, where u_i' is the subgrid gas velocity. $F_i = \left(\sum_d F_{i,d}\right) V_{cell}$ is the aerodynamic drag force. In this study, the definition of the subgrid gas velocity is $u_i' \equiv u_i - \tilde{u}_i$, where the tilde represents the box filter. So the above equation can be re-written as $\overline{\dot{W}^s} \equiv -\left(\sum_d F_{i,d} u_i'\right) V_{cell}$. After two test filtering procedures, the subgrid gas velocity can be written simply as $u_i' = 2\tilde{u}_i - 3\tilde{\tilde{u}}_i + \tilde{\tilde{\tilde{u}}}_i$, where the number of tildes represents the number of filtering operations. So the final form of the spray source term can be written as $\overline{\dot{W}^s} = -\frac{3}{8}\frac{C_D}{V_{cell}} \sum_d \{\frac{m_d \rho V_{rel}}{r_d \rho_l} \left(\tilde{u}_i + u'_{p,i} - v_{d,i}\right) \left(2\tilde{u}_i - 3\tilde{\tilde{u}}_i + \tilde{\tilde{\tilde{u}}}_i\right)\}$. A more detailed derivation of the spray source term can be found in [46].

2.3 Dynamic adaptive chemistry

With DAC, the full set of chemical species in a mechanism are transported in the simulations. Chemical reaction process is separated from other physical processes such as diffusion and advection, and being solved in reaction fractional steps, in which the compositions $\Phi \equiv \{\mathbf{Y}, \mathbf{h_s}\}$, where $\mathbf{Y}$ stands for the n_s-vector of species mass fraction Y_i, h_s the mixture sensible enthalpy, are governed by a set of $n_s + 1$ nonlinear stiff ODEs

$$\frac{d\Phi}{dt} = \mathbf{S}(\Phi), \tag{8}$$

where $\mathbf{S}$ is the source term due to chemical reactions. Given an initial composition, the time-evolving solution corresponds to a reaction trajectory in the composition space. With DAC, at the beginning of each reaction fractional step, for each CFD cell, a small skeletal mechanism valid for the local thermo-chemical condition based on a pre-specified reduction error threshold is obtained by eliminating unimportant species Φ^u and reactions. Thus only a small subset of species Φ^r and reactions in the full mechanism are retained to capture the dominant reaction pathways for each local thermo-chemical condition. The DAC approach accelerates the time-integration of the reaction substeps by approximating the unimportant species to be chemically frozen during the integration time step and solving only the non-trivial ODEs governing the retained species together with mixture sensible enthalpy, as the following equations:

$$\frac{d\Phi^r}{dt} = \mathbf{S^r}(\Phi) \frac{\mathbf{d}\Phi^\mathbf{u}}{\mathbf{dt}} = \mathbf{0} \tag{9}$$

where $\mathbf{S^r}$ is the chemical source term for the retained species. More details of DAC can be found in the Refs.[30, 35, 52].

In this study the DRG method [35] is implemented for species and reaction removal. For a given cell composition, it determines the unimportant species that do not significantly affect the reaction rates of the major species based on a threshold, ε_{DAC} , for the truncation of weak species couplings. The search-initiating species in DRG are taken to be three non-inert species dynamically selected based on abundance in mass fraction together with three user-specified species, i.e. CO, H, and NO. Note that the user-specified species will be replaced as dynamically selected ones once the mass fraction approaches zero. This automatic procedure avoids the ambiguity in the fixed species strategies when the concentrations of one (or more) specified search-initiating species approach zero and can dynamically select the species of importance based on the progress of the combustion process. The inclusion of

CO and NO as searching-initiating species can effectively ensure the prediction accuracy in CO and NO. It is worth mentioning that the reduction threshold ε_{DAC} effectively controls the locally incurred errors in composition by DAC in the reaction substeps. In addition, solution convergence with the DAC reduction threshold has been extensively investigated in zero-dimensional or (U)RANS simulations [29, 30, 32, 34, 53], showing that the results calculated with DAC approach the ones without DAC, as the DAC reduction threshold decreases.

2.4 Numerical settings

The computational domain is set to be a cylindrical geometry being 30 mm in diameter and 100 mm in height. The 3D grids employed having 90,000 cells (coarse grid) for URANS and 720,000 cells (fine grid) for LES as shown in Fig. 1, are based on previous studies of Bharadwaj et al. [46], Hori et al. [54], and Zhou et al. [55]. The time step varies from 1.0×10^{-8} s to 1.0×10^{-6} s, depending on physicochemical time scales and the CFL number in the simulations. No-slip adiabatic wall boundary conditions are applied to all the boundaries except the injection section. The injection and operation conditions [3] are set to be the same as those in the experiment, as listed in Table 1.

In the simulations, the initial droplet diameter is assumed to be equal to the orifice diameter. A stochastic parcel method is adopted to reproduce the spray behaviors with each parcel represents the droplets having the same fuel mass, size and motion. In this work, the number of spray parcels to be injected is 40,000 for both LES and URANS. The droplets are

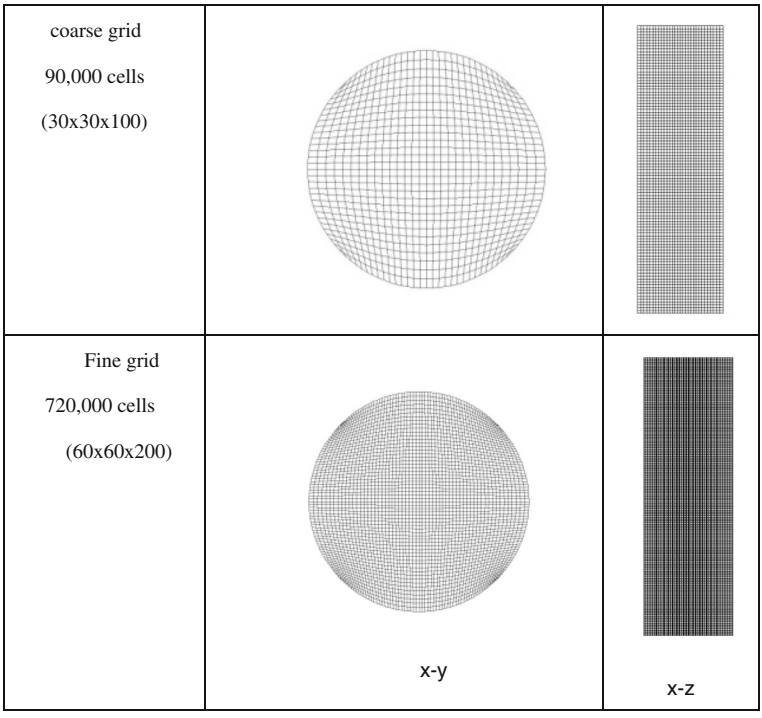

Fig. 1 The uniform computational meshes : the size of coarse grid is 1.0 mm and the size of fine grid is 0.5 mm

Table 1 Experimental conditions

Injected fuel	C_7H_{16}
Orifice diameter (mm)	0.1
Injection duration (ms)	6.8
Injection pressure (MPa)	150
Fuel mass (mg)	17.8
Fuel temperature (K)	373
O_2 (vol. %)	0%(non-reaction) 21%(reaction)
Ambient density (kg/m^3)	14.8
Ambient temperature (K)	1000

injected continuously one after another according to the given fuel mass flow rate during the injection process. The liquid density is 684 kg/m^3.

In addition to DAC, a uniformly random distribution parallelization algorithm [56] is implemented to further facilitate the chemistry calculations. As for the parallelization strategy, the fluid dynamics is solved on a single processor, while chemistry calculations are performed on 24 processors (Intel Xenon X5670 with 2.93GHz and 12MB cache).

The predicted flow and combustion characteristics such as liquid/gas penetration, ignition delay time, flame LOL and emissions are investigated. The ignition delay time and LOL in this study are defined as in [9]. Specifically, the ignition delay time is defined as the time after the start of injection (ASI) when the highest temperature over the entire computational domain reaches the ignition temperature defined as $T_{ign} = (T_{amb} + T_{max})/2$, where T_{amb} is the ambient temperature and $T_{\max}$ is the highest temperature that can occur in the flame during the entire combustion process. The LOL is defined as the axial distance between the inlet and the most upstream point with $T = T_{ign}$.

3 Flow and Combustion Characteristics

3.1 Effect of spray and turbulence modelling on flow characteristics

The non-reacting spray process is first simulated with URAN to investigate the effects of spray modelling on the penetration characteristics of the "Spray H". The ambient oxygen concentration is 0 % and other simulation conditions are listed in Table 1. Figure 2 shows the calculated and experimental evolutions of the liquid and vapor penetration versus time after start of injection. The liquid penetration is defined as the axial location where 95 % of the droplets mass stays in the upstream side. The vapor penetration is determined by the farthest downstream location of 0.1 % fuel mass fraction. As shown, URANS without gas-jet model apparently under-predicts the vapor penetration, while the fine grid case has a small shift towards the experiment results. In contrast, the simulations with gas-jet model show good agreement with the experimental data. More importantly, as illustrated by the results from the two set of grids, the gas penetration and fuel distribution predicted by the URANS simulations with gas jet model shows weak dependence on the grid resolution. As

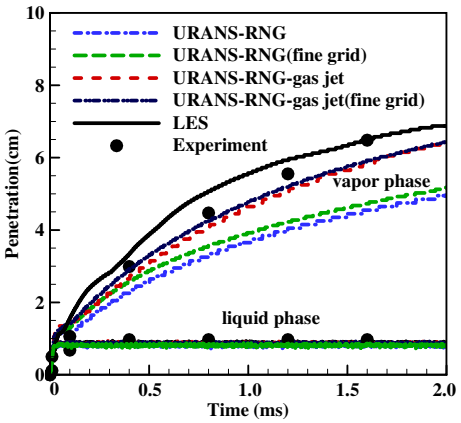

Fig. 2 The calculated and experimental evolutions of the liquid and vapor penetrations versus time after the start of injection. The turbulent model for URANS is the RNG $k-\varepsilon$ model

for the liquid phase penetration length, the simulation results from different methods all agree well with the experimental data. For the case simulated, the ambient temperature is much higher than the fuel boiling point. The liquid penetration length is dominated by the evaporation process since the liquid droplets vaporizes very quickly after injection into the chamber. Therefore, the spray models do not have significant influence on its prediction.

To illustrate the effects of turbulence modelling on the penetration characteristics, Fig. 3 shows the liquid and vapor penetrations profile from the standard $k-\varepsilon$ model. Again the prediction of the vapor penetration length is improved by the gas jet model. And the simulations with gas jet model have weaker dependence on the grid density. In addition, large eddy simulations are also performed on the fine grid of 720,000 cells. As shown in Fig. 2, although the gas-jet model is not employed in LES, the transient behavior of the vapor penetration length observed in experiment is still well reproduced. The reason is that the LES accurately resolves the large bulk motion, leading to a reasonable gas velocity directly as discussed in previous studies [45, 57].

To further quantify the impact of gas jet model on the gas-phase velocity and fuel distributions, Figs. 4 and 5 compare the calculated velocity and mixture fraction from URANS

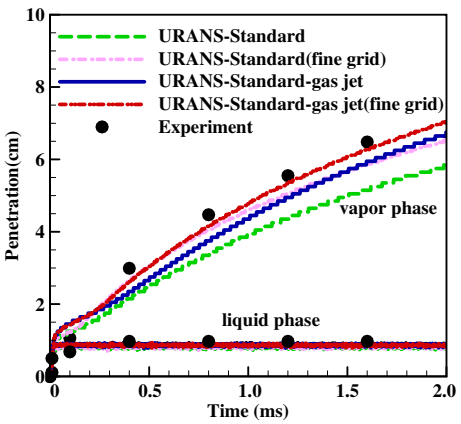

Fig. 3 The calculated and experimental evolutions of the liquid and vapor penetrations versus time after the start of injection using the standard $k-\varepsilon$ model

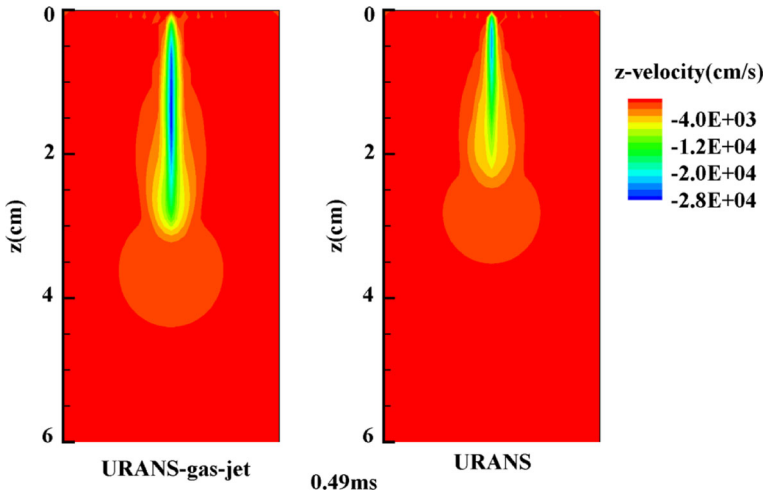

Fig. 4 The calculated gas-phase z-velocity distributions from URANS simlations with/without gas jet model at 0.49 ms ASI on the coarse mesh

simulations with the RNG $k-\varepsilon$ model and the standard $k-\varepsilon$ model. As shown, the gas-jet model yields significantly larger axial velocities in the region between the nozzle and z=2 cm downstream position, where fuel vapor concentrates. The original model takes the gas velocity of the grid cell directly as the gas-liquid relative velocity in Eq. 5 and therefore it cannot yield the accurate relative velocity, leading to non-physical high resistance or drag force effects. Consequently, the droplet velocity is reduced, which eventually affects the gas phase velocity through the momentum exchange between the two phases. As for the gas-jet model, the relative velocity is modelled based on the solution of a gas phase jet flow, making the drag force close to the realistic case. The difference in the gas-phase velocity has profound effects on the fuel distributions. Figure 5 shows the mixture fraction profiles from three axial locations at 0.49 ms and 6 ms ASI. As shown, at z=1 cm, the mixture fraction predicted with gas-jet model is lower than that without gas-jet model, resulting from the larger axial velocity with the gas-jet model taking more fuel vapor downstream. It is also observed that the fuel distributions at 0.49 ms and 6.0 ms ASI are close to each other, implying that the injection process approaches statistically stationary quickly. For further downstream locations of z=1.7 cm at 0.49 ms ASI and z=2.0 cm at 6.0 ms ASI where experimental data are available, it is observed that the gas-jet model in general improves the predictions, while the URANS without the gas-jet model yields a much wider fuel distribution due to the smaller convective transport at the streamwise direction. Note that even with the gas-jet model, the standard $k-\varepsilon$ model yields significantly wider fuel distribution at z=1.7 cm during the early transient state. It is worth mentioning that the computed mixture fraction is also sensitive to other model parameters such as turbulent Schmidt number, break-up model parameters, whose effects are subject to future study. In the present study a default turbulent Schmidt number of 0.9 is employed, while reducing it may improve the mixture fraction prediction.

In summary, for the case considered, the liquid penetration length dominated by the evaporation process is insensitive to the spray modelling, while the droplets motions near the nozzle has significant influence on the fuel vapor distribution. For URANS, the gas-jet

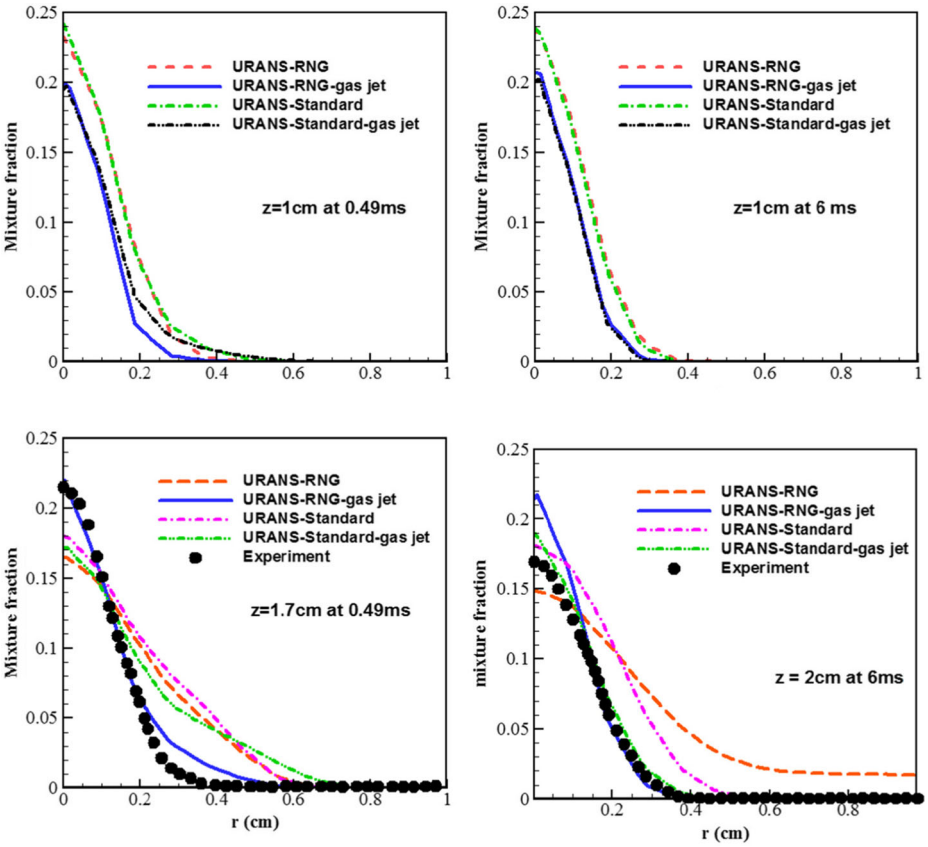

Fig. 5 The calculated and experimental radial profiles of mixture fraction at different axial locations and time instances from the URANS simulations using the RNG model and the standard $k-\varepsilon$ model with and without gas jet model on the coarse grid. Left column: 1.7 cm and 1.0 cm at 0.49 ms ASI; right column: 1.0 cm and 2.0 cm at 6.0 ms ASI

model can significantly increase the vapor penetration and therefore improve the prediction of fuel distribution.

3.2 Effect of spray and turbulence modelling on combustion characteristics

To quantify the effect of spray and turbulence modelling on the combustion characteristics, the predicted instantaneous flame structures, ignition delay time and flame LOL are investigated. Figure 6 illustrates the apparent differences in temperature distributions from URANS, URANS with gas jet model and LES at $t=2.0$ ms ASI. As shown for URANS, the gas jet model significantly increases the high-temperature area and therefore the flame length as a result of larger vapor penetration (see Fig. 2). The predicted flame length and LOL from URANS with gas jet model are comparable to the ones from LES, even though the latter captures more detailed flame structures.

To further quantify the global combustion characteristics from the different methods, Fig. 7 shows the quantitative comparison of the predicted ignition delay times and flame

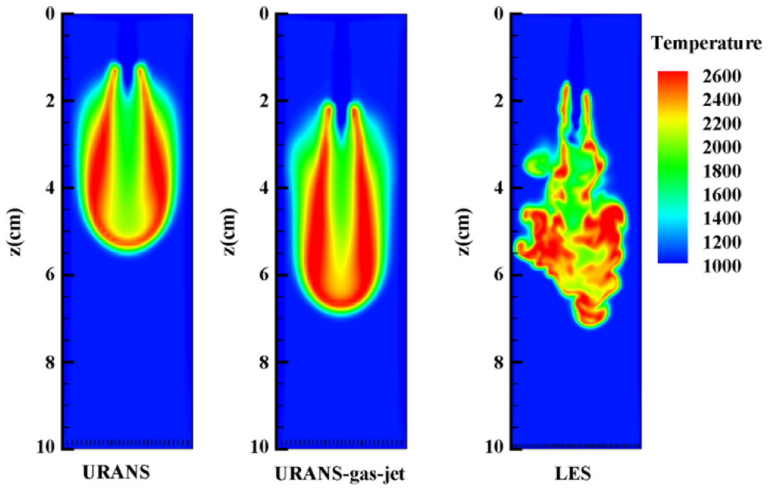

Fig. 6 The instantaneous temperature distributions from different methods at $t = 2.0$ ms ASI for the case $T_{amb} = 1000$ K. The URANS simulations are performed on the coarse grid of 90,000 cells and the LES is from the fine grid of 720,000 cells

lengths. The flame length is defined to be the distance from the position of flame lift-off length to the flame tip. As shown, LES yields the best predictions in the global combustion characteristics compared to the experimental data. For the URANS, the gas jet model yields a larger ignition delay time compared to the experimental data, although it results in an improved prediction in the flame length.

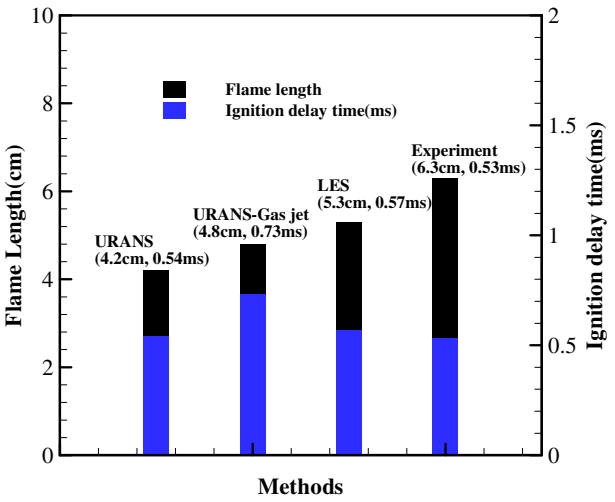

Fig. 7 The predicted ignition delay times and flame lengths from different methods at $t = 2.0$ ms ASI for the case $T_{amb} = 1000$ K

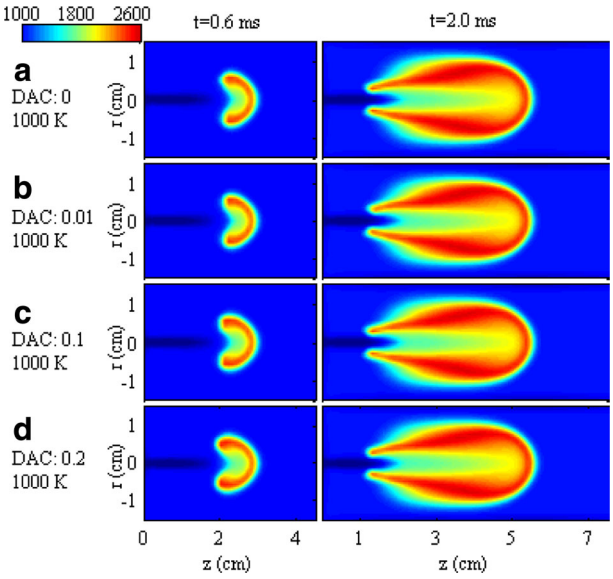

Fig. 8 Temperature distributions with different values of ε_{DAC} at $t = 0.6$ ms and $t = 2.0$ ms for $T_{amb} = 1000$ K from URANS

4 Solution Convergence with Chemistry Reduction Threshold

To facilitate the detailed chemistry calculations, dynamic adaptive chemistry is employed in the calculations. As illustrated in the above, large eddy simulations yield the best predictions in the combustion characteristics. However, the convergence characteristics with

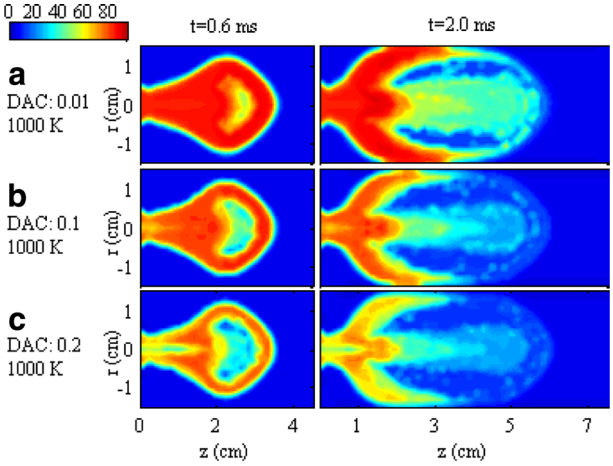

Fig. 9 The number of important species with different values of ε_{DAC} at $t = 0.6$ ms and $t = 2.0$ ms for $T_{amb} = 1000$ K from URANS

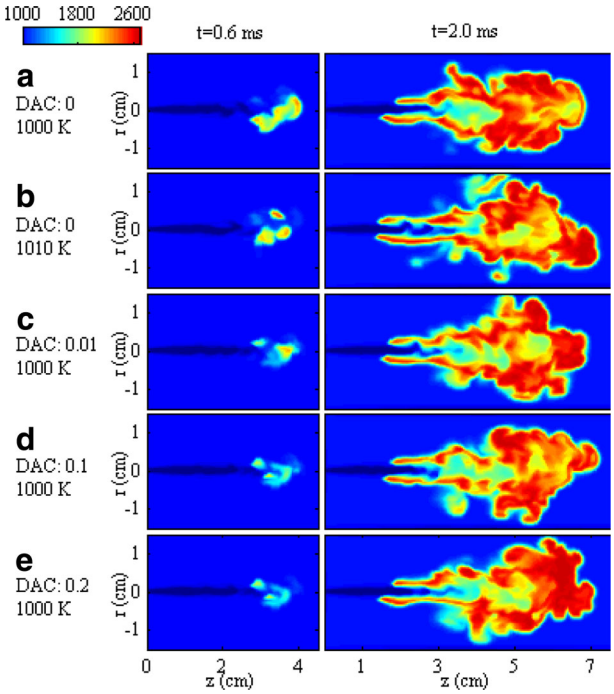

Fig. 10 Temperature distributions with different values of ε_{DAC} and ambient temperature T_{amb} at $t = 0.6$ ms and $t = 2.0$ ms, respectively. **a** Full description without DAC, $T_{amb} = 1000$ K; **b** full description without DAC, $T_{amb} = 1010$ K; **c** to **e** descriptions for $T_{amb} = 1000$ K. with $\varepsilon_{DAC} = 0.01, 0.1, 0.2$, respectively

respect to the DAC reduction threshold have not been analysed thoroughly for the transient simulations, especially LES. To achieve so, transient simulations of "Spray H" with different values of ε_{DAC} are performed to investigate the effect of DAC on the predicted instantaneous flame structures and ignition delay time, flame LOL and emissions. The presented URANS results are from the ones without gas-jet model to focus on investigating the convergence difference between LES and URANS without the influence of the spray model, even though the gas jet model does not affect the solution convergence characteristics with chemistry reduction threshold. For comparison, simulation without DAC ($\varepsilon_{DAC} = 0$) is also performed. Several time instances such as $t = 0.6$ ms and $t = 2.0$ ms, corresponding to the stages of start of ignition and fully developed combustion, are analysed.

4.1 Convergence characteristics of URANS-DAC

Three different thresholds, $\varepsilon_{DAC} = 0.01$, 0.1, and 0.2, are employed to investigate the errors associated with DAC, comparing with results without DAC application. Figures 8 and 9 show the temperature contour plots and the numbers of retained important species at different time instances. As expected, an increased ε_{DAC} significantly reduces the number of retained species since more species couplings are truncated. Note that for the three values of ε_{DAC} considered, the temperature distributions have no noticeable difference, even though the maximum number of retained species has been reduced from 92 for $\varepsilon_{DAC} = 0.01$ to 75 for $\varepsilon_{DAC} = 0.2$. It is further noted that the number of retained species peaks at the flame

base, rather than the locations with highest temperatures, where the mixture is near chemical equilibrium. Here the flame base is defined to be the point with the axial position $z = \text{LOL}$, and its temperature satisfies $T\ (z,\ r) = T_{ign}$, where r is the radial coordinate. As shown, there is no noticeable difference in LOL among the URANS simulations with and without DAC.

4.2 Convergence characteristics of LES-DAC

LES directly resolves the large-scale unsteady motions in "Spray H". It is straightforward to investigate the effect of DAC on the instantaneous flame structures by comparing the predicted temperature distributions (at the same time) from different values of ε_{DAC} , as shown in Fig. 10. Note that the "random" number sequences are the same in all LES simulations, and the differences in the flame structures are incurred by DAC only. As shown, with the same ambient temperature ($T_{amb} = 1000\,\text{K}$), there are noticeable differences in the instantaneous flame structures from the calculations with $\varepsilon_{DAC} = 0\ (no\ DAC)\,0.01,\ 0.1,\ 0.2$ respectively, although the overall flame shapes and the global parameter flame LOL are similar. This is dramatically different from the URANS simulations as shown in Fig. 8 where the solution convergence with the DAC reduction threshold is demonstrated by showing that there are no noticeable differences in temperature distributions from the calculations with and without DAC.

The different DAC convergence characteristics between URANS and LES are due to the strong coupling between chemical reactions and flow field. The errors in species evolution and heat release, induced by the elimination of species and reactions in DAC during the reaction substeps, may alter the local small flow structures through the coupling of density. To illustrate the sensitivity of the instantaneous flame structure to perturbations, a LES

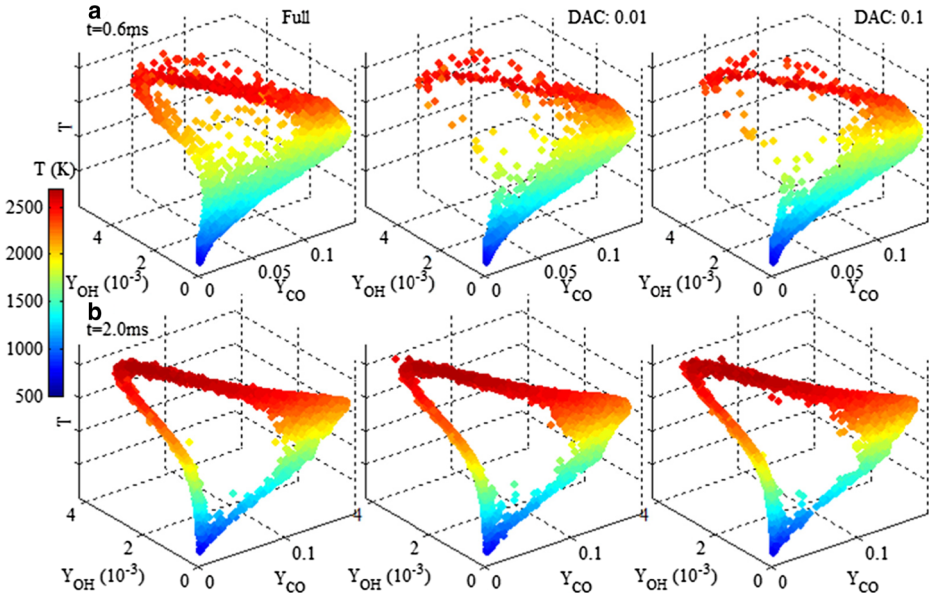

Fig. 11 Distribution of sample compositions in $\text{CO} - \text{OH} - T$ subspace, colored by temperature at $t = 0.6$ ms and $t = 2.0$ ms ASI, respectively

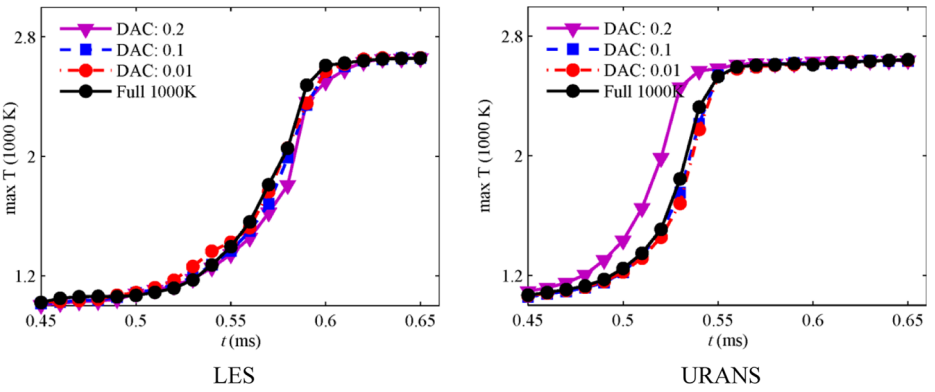

Fig. 12 The evolution of maximum temperature in the whole computational domain from LES and URANS calculations with different DAC error tolerances

calculation with T_{amb}= 1010 K (Case b in Fig. 10) is performed to illustrate the effect of experimental uncertainty in ambient temperature on instantaneous flame structure. The 10 K displacement in T_{amb} is reasonable regarding the fact that T_{amb} is a normal distribution with a standard deviation of 2.1 % of the mean in experiment [3]. As shown, the 10 K difference in T_{amb} significantly affect the auto-ignition process and consequently the flame structure. As a comparison, the effect of the 10K difference in ambient temperature on flame structure and LOL is more significant than the use of DAC. The above analysis implies that in LES context a convergence study of DAC should not be based on the comparison of local instantaneous quantities or fields such as flame structure and species distributions since they may be very sensitive to small perturbations such as the one incurred by DAC. In the following, manifolds in composition space, conditional quantities and some global quantities are proposed to assess the LES-DAC results.

To focus on investigating the effect of DAC on instantaneous compositions, Fig. 11 shows the projection of sample compositions from two time instances in the major intermediate species CO, crucial radical OH, and temperature T subspace. By exploring the flame structure in the composition space, the subtle effect of flow field on the flame structure in physical space as shown in Fig. 10 is removed. For t = 0.6 ms, all the cell compositions in the reactive region are presented and for t = 2.0 ms ten thousands cell composition are

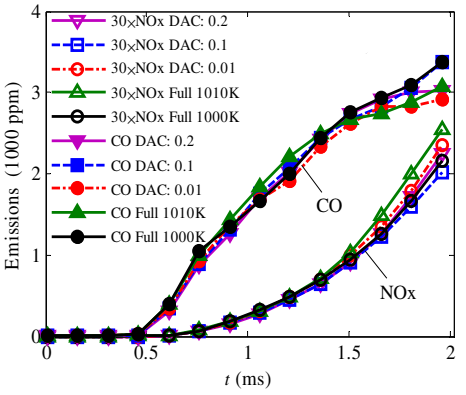

Fig. 13 The mean CO and NOx mass fraction in the whole computational domain from LES calculation with different DAC error tolerances

randomly picked in the reactive region. Here the reactive region is defined as $T \geq 1050$ K, $Y_{OH} \geq 0.001$, and $Y_{CO} \geq 0.01$. It is seen that the distributions of CO, OH, and T form curved surfaces in the three-dimensional subspace. In the reactive region, liquid fuel at a low temperature of 373 K is injected into the air of 1000 K. At $t = 0.6$ ms, a large number of points are with low temperature, showing the mixing and start of ignition, while at $t = 2.0$ ms, when the flame is fully developed, most sample points lie in high temperature region as expected. As shown, DAC do not have significant influence on the manifold in composition space although the instantaneous flame structure in physical space is dramatically different as shown in Fig. 10. The subtle difference is that at $t = 0.6$ ms the full description has more composition samples with high temperature, resulting a slight earlier ignition than the descriptions with DAC (see Fig. 12) and consequently a larger flame area (see Fig. 10).

4.3 Global combustion characteristics

The effect of DAC on global combustion characteristics such as flame lift-off length (LOL), ignition delay time and emissions are investigated below. As shown, the agreement in ignition delay and LOL between descriptions with and without DAC improves when the DAC threshold decreases. While URANS predicts ignition delay well, it gives large errors in LOL compared with experimental data. The error on LOL predicted by URANS is likely to be induced by the poorly resolved flow fields without the gas-jet model. For the LES where the flow field is better solved, closer predictions of the LOL are observed. Even with the biggest threshold considered, e.g. $\varepsilon_{DAC} = 0.2$, the relative error in LOL is less than 4 %, which is far less than the error (9.7 %) incurred by the 10 K displacement in T_{amb}.

The ignition characteristics from different descriptions are studied by comparing the evolutions of the maximum temperature over the entire computational domain as shown in Fig. 12. For all the three values of ε_{DAC} considered using LES, the maximum temperature profiles agree well with the one without DAC. The relative errors in ignition delay times are 1.7 %, 1.0 %, 0.2 % for $\varepsilon_{DAC} = 0.2,\ 0.1,\ 0.01$, respectively. In comparison, for URANS a shift on the maximum temperature prediction from the full description is observed for $\varepsilon_{DAC} = 0.2$, resulting in approximately a 5 % error in ignition delay time, while the error vanishes with reduced ε_{DAC} The emission characteristics such as the evolution of mean CO and NOx concentrations over the entire computational domain from LES simulations are presented in Fig. 13. Once again it is observed that for the three values of ε_{DAC} considered, the errors incurred by DAC are small and they are comparable to the one incurred by 10 K uncertainty in T_{amb}.

Table 2 The lift-off length, ignition delay, and computational speedup for the cases $T_{amb} = 1000$ K with different values of ε_{DAC} for URANS and LES

	Exp.	URANS No DAC	URANS $\varepsilon_{DAC} = 0.01$	URANS $\varepsilon_{DAC} = 0.1$	URANS $\varepsilon_{DAC} = 0.2$	LES No DAC	LES $\varepsilon_{DAC} = 0.01$	LES $\varepsilon_{DAC} = 0.1$	LES $\varepsilon_{DAC} = 0.2$
LOL(cm)	1.7	1.20	1.20	1.20	1.20	1.55	1.55	1.60	1.50
Ignition delay(ms)	0.53	0.54	0.53	0.53	0.52	0.57	0.57	0.58	0.58
Speedup	N/A	1.0	1.40	1.79	2.08	1.0	1.70	1.99	2.19

Computation efficiency improvement by DAC is also listed in Table 2, normalized by the full description calculation cost. Note that the chemistry calculation is the dominant part in all these calculations and the flow computation accounts for less than 4 % of the overall simulation time. A speedup factor of about 2 is achieved by the application of the DAC with $\varepsilon_{DAC} = 0.1$, which is substantial considering that the 88-species n-heptane mechanism employed has already been greatly reduced from the detailed 561-species mechanism.

5 Conclusions

Unsteady Reynolds-averaged Navier-Stokes simulations and large eddy simulations are performed to investigate the effects of spray and turbulence modelling on the mixing and combustion characteristics of the "Spray H" flame. The entrainment gas-jet model as an improved liquid spray model has been incorporated in the URANS to improve the predictions in liquid and gas penetrations. For the non-reacting spray process case considered, URANS without gas-jet model show larger grid dependence and may under-predicts the vapor penetration and therefore poor prediction in mixture fraction on coarse grid due to the under-predicted low gas phase velocity. In contrast, the URANS simulation with gas-jet model show less grid-dependence and achieves better predictions on both penetration and fuel vapor distributions by improving the estimation of the gas-liquid relative velocity. For the case considered, the droplets motion near the nozzle has significantly influence on the fuel vapor distributions, while the liquid penetration length is dominated by the evaporation process and insensitive to the spray and turbulence modelling. URANS simulations with the gas-jet model and large eddy simulations can properly predict the vapor penetration. Basically the gas-jet model has similar effects for both RNG and standard $k-\varepsilon$ model cases in URANS. As for the combustion characteristics, LES yields the best predictions in the global combustion characteristics. The URANS with gas jet model yields a comparable flame length and lift-off-length to LES, but results in a larger ignition delay time compared to the experimental data.

To assess the solution convergence characteristics with DAC for transient simulations, the instantaneous flame structures and global combustion characteristics such as ignition delay time, flame lift-off length and emissions from URANS and LES are investigated. For the three reduction threshold values considered, it is observed that there are dramatic differences in the instantaneous flame structures from the LES simulations with and without DAC, which is different from the observations made in URANS simulations where the differences in flame structures are small and decrease with the DAC reduction threshold. The different DAC convergence characteristics between URANS and LES are due to the strong coupling between chemical reactions and flow field. The errors in species evolution and heat release, induced by the elimination of species and reactions in DAC during the reaction sub-steps, may alter the local small-scale flow structures through the coupling of density in LES, but not in URANS where these stochastic local small disturbances are averaged out at all length scales. The study reveals that in the LES context, appraisal of the effect of DAC on solution accuracy should not be solely based on the local instantaneous quantities or fields such as flame structure and species distributions since they may be sensitive to small perturbations incurred by DAC. More importantly, manifolds in composition space, conditional quantities and global combustion characteristics need to be used to assess the LES-DAC results.

For the three reduction threshold values considered, it was found that the scatter distribution in composition space and conditional means from descriptions with and without

DAC are similar even though the instantaneous flame structure in physical space is dramatically different. This implies DAC has no significant effect on the reaction trajectories in the composition space. The effect of DAC on global combustion characteristics such as flame lift-off length, ignition delay time and emissions are assessed. It is found that the agreement in LOL between descriptions with and without DAC improves when the DAC threshold decreases. Even with the biggest threshold value considered, e.g. $\varepsilon_{DAC} = 0.2$, the relative error in LOL is less than 4 %, which is far less than the error (9.7 %) incurred by the 10 K uncertainty in T_{amb}. The ignition and emission characteristics from different descriptions are also studied by comparing the evolutions of the maximum temperature, mean CO and NOx concentrations over the entire computational domain. For all the three values of ε_{DAC} considered, the errors incurred by DAC are small and are comparable to those incurred by the 10 K uncertainty in T_{amb}. As far as computational efficiency is concerned, a speed-up factor of more than two is achieved by DAC with the already highly reduced 92-species skeletal mechanism.

Acknowledgments The work is supported by National Natural Science Foundation of China (91441202, 51476087) and the China Postdoctoral Science Foundation (2012M510437). The parallel supercomputer at the Tsinghua National Laboratory for Information Science and Technology is used for the simulations. The work at UConn was supported by the Office of Basic Energy Sciences, Office of Science, U.S. Department of Energy under Grant DE-SC0008622.

References

1. Jiang, X., Siamas, G.A., Jagus, K., Karayiannis, T.G.: Physical modelling and advanced simulations of gas–liquid two-phase jet flows in atomization and sprays. Prog. Energy Combust. Sci. **36**, 131–167 (2010)
2. Idicheria, C.A., Pickett, L.M.: Effect of EGR on diesel premixed-burn equivalence ratio. Proc. Combust. Inst. **31**(2), 2931–2938 (2007)
3. Pickett, L., Bruneaux, G.: Engine combustion network, Combustion research facility, Sandia national laboratories, Livermore, CA. See http://www.sandia.gov/ECN (2011)
4. Zhou, L., Luo, K.H., Qin, W., Jia, M., Shuai, S.J.: Large eddy simulation of spray and combustion characteristics with realistic chemistry and high-order numerical scheme under diesel engine-like conditions. Energy Convers. Manag. **93**(0), 377–387 (2015)
5. Zhou, L., Ren, Z., Lu, Z., Lu, T., Luo, K.: Large-eddy simulations of an n-heptane spray flame with dynamic adaptive chemistry. SAE Int. J. Engines **8**(2), 447–454 (2015)
6. Pei, Y., Hawkes, E.R., Kook, S.: Transported probability density function modelling of the vapour phase of an n-heptane jet at diesel engine conditions. Proc. Combust. Inst. **34**(2), 3039–3047 (2013)
7. Bhattacharjee, S., Haworth, D.C.: Simulations of transient n-heptane and n-dodecane spray flames under engine-relevant conditions using a transported PDF method. Combustion and Flame **160**(10), 2083–2102 (2013)
8. Som, S., Longman, D.E., Luo, Z., Plomer, M., Lu, T., Senecal, P.K., Pomraning, E.: Simulating flame lift-off characteristics of diesel and biodiesel fuels using detailed chemical-kinetic mechanisms and large eddy simulation turbulence model. J. Energy Resour. Technol. **134**(3), 1–10 (2012)
9. Bekdemir, C., Somers, L.M.T., de Goey, L.P.H., Tillou, J., Angelberger, C.: Predicting diesel combustion characteristics with Large-Eddy Simulations including tabulated chemical kinetics. Proc. Combust. Inst. **34**(2), 3067–3074 (2013)
10. Bottone, F., Kronenburg, A., Gosman, D., Marquis, A.: The numerical simulation of diesel spray combustion with LES-CMC. Flow, Turbul. Combust. **89**(4), 651–673 (2012)
11. Vishwanathan, G., Reitz, R.D.: Development of a practical soot modeling approach and its application to low-temperature diesel combustion. Combust. Sci. Technol. **182**(8), 1050–1082 (2010)
12. Lucchini, T., d'Errico, G., Ettorre, D., Ferrari, G.: SAE technical paper (2009)
13. Azimov, U., Kim, K.-S., Bae, C.: Modeling of flame lift-off length in diesel low-temperature combustion with multi-dimensional CFD based on the flame surface density and extinction concept. Combustion Theory and Modelling **14**(2), 155–175 (2010)

14. Zhou, L., Lu, Z., Ren, Z., Lu, T., Luo, K.: Numerical analysis of ignition and flame stabilization in an n-heptane spray flame, International Journal of Heat and Mass Transfer **88**, 565–571 (2015)
15. Post, S., Iver, V., Abraham, J.: A study of near-field entrainment in gas jets and sprays under diesel conditions. J. Fluids Eng. **122**(2), 385–395 (2000)
16. Beard, P., Duclos, J.-M., Habchi, C., Bruneaux, G., Mokaddem, K., Baritaud, T.: Extension of Lagrangian-Eulerian spray modeling: application to high-pressure evaporating diesel sprays. SAE Trans. **109**(4), 1417–1434 (2000)
17. Beard, P., Colin, O., Miche, M.: Improved modelling of DI diesel engines using sub-grid descriptions of spray and combustion. SAE Trans. **112**(3), 73–86 (2003)
18. Abraham, J.: Entrapment characteristics of transient gas jets. Numerical Heat Transfer Part A Applications **30**(4), 347–364 (1996)
19. Curran, H.J., Gaffuri, P., Pitz, W.J., Westbrook, C.K.: A comprehensive modeling study of iso-octane oxidation. Combustion and Flame **129**(3), 253–280 (2002)
20. Curran, H.J., Gaffuri, P., Pitz, W.J., Westbrook, C.K.: A comprehensive modeling study of n-heptane oxidation. Combustion and Flame **114**(1–2), 149–177 (1998)
21. Lu, T., Law, C.K.: Toward accommodating realistic fuel chemistry in large-scale computations. Prog. Energy Combust. Sci. **35**(2), 192–215 (2009)
22. Pope, S.B.: Small scales, many species and the manifold challenges of turbulent combustion. Proc. Combust. Inst. **34**(1), 1–31 (2013)
23. Pope, S.B., Ren, Z.: Efficient implementation of chemistry in computational combustion. Flow, Turbulence and Combustion **82**(4), 437–453 (2009)
24. Bilger, R., Pope, S., Bray, K., Driscoll, J.: Paradigms in turbulent combustion research. Proc. Combust. Inst. **30**(1), 21–42 (2005)
25. Law, C.K.: Combustion physics. Cambridge University Press, New York (2006)
26. Peters, N.: Turbulent combustion. Cambridge University Press (2000)
27. Tomlin, A.S., Turányi, T., Pilling, M.J.: Mathematical tools for the construction, investigation and reduction of combustion mechanisms. Comprehensive chemical kinetics **35**, 293–437 (1997)
28. Warnatz, J., Maas, U., Dibble, R.W.: Combustion: Physical and chemical fundamentals, modeling and simulation, experiments, pollutant formation: Springer (2006)
29. Liang, L., Stevens, J.G., Farrell, J.T.: A dynamic adaptive chemistry scheme for reactive flow computations. Proc. Combust. Inst. **32**(1), 527–534 (2009)
30. Yang, H., Ren, Z., Lu, T., Goldin, G.M.: Dynamic adaptive chemistry for turbulent flame simulations. Combustion Theory and Modelling **17**(1), 167–183 (2013)
31. Liang, L., Stevens, J.G., Raman, S., Farrell, J.T.: The use of dynamic adaptive chemistry in combustion simulation of gasoline surrogate fuels. Combustion and Flame **156**(7), 1493–1502 (2009)
32. Shi, Y., Liang, L., Ge, H.-W., Reitz, R.D.: Acceleration of the chemistry solver for modeling DI engine combustion using dynamic adaptive chemistry (DAC) schemes. Combustion Theory and Modelling **14**(1), 69–89 (2010)
33. Tosatto, L., Bennett, B.A.V., Smooke, M.D.: A transport-flux-based directed relation graph method for the spatially inhomogeneous instantaneous reduction of chemical kinetic mechanisms. Combustion and Flame **158**(5), 820–835 (2011)
34. Contino, F., Foucher, F., Dagaut, P., Lucchini, T., D'Errico, G., Mounaïm-Rousselle, C.: Experimental and numerical analysis of nitric oxide effect on the ignition of iso-octane in a single cylinder HCCI engine. Combustion and Flame **160**(8), 1476–1483 (2013)
35. Lu, T., Law, C.K.: A directed relation graph method for mechanism reduction. Proc. Combust. Inst. **30**(1), 1333–1341 (2005)
36. Lu, T., Law, C.K.: On the applicability of directed relation graphs to the reduction of reaction mechanisms. Combustion and Flame **146**(3), 472–483 (2006)
37. Pepiot-Desjardins, P., Pitsch, H.: An efficient error-propagation-based reduction method for large chemical kinetic mechanisms. Combustion and Flame **154**(1–2), 67–81 (2008)
38. Sun, W., Chen, Z., Gou, X., Ju, Y.: A path flux analysis method for the reduction of detailed chemical kinetic mechanisms. Combustion and Flame **157**(7), 1298–1307 (2010)
39. Oluwole, O.O., Ren, Z., Petre, C., Goldin, G.: Decoupled species and reaction reduction: An error-controlled method for dynamic adaptive chemistry simulations. Combustion and Flame **162**(5), 1934–1943 (2015)
40. Alamos, L.: KIVA-3V: A block-structured Kiva program for engines with vertical or canted values.LA-18818-MS,1997
41. Van Leer, B.: Towards the ultimate conservative difference scheme. II. Monotonicity and conservation combined in a second-order scheme. J. Comput. Phys. **14**(4), 361–370 (1974)

42. Sone, K., Menon, S.: Effect of subgrid modeling on the in-cylinder unsteady mixing process in a direct injection engine. J. Eng. Gas Turbines and Power-Transactions of the Asme **125**(2), 435–443 (2003)
43. Patterson, M.A., Reitz, R.D.: Modeling the effects of fuel spray characteristics on diesel engine combustion and emission. Fuel **1998**, 09–05 (2013)
44. O'Rourke, P.J.: Collective drop effects on vaporizing liquid sprays: Princeton University (1981)
45. Zhou, L., Xie, M.Z., Jia, M.: Influences of subgrid turbulent kinetic energy and turbulent dispersion on the characteristics of fuel spray, SAE: 2011-01-1839 (2011)
46. Bharadwaj, N., Rutland, C., Chang, S.: Large eddy simulation modelling of spray-induced turbulence effects. Int. J. Eng. Res. **10**(2), 97–119 (2009)
47. Yoo, C.S., Lu, T., Chen, J.H., Law, C.K.: Direct numerical simulations of ignition of a lean n-heptane/air mixture with temperature inhomogeneities at constant volume: Parametric study. Combustion and Flame **158**(9), 1727–1741 (2011)
48. Li, Y., Jia, M., Liu, Y., Xie, M.: Numerical study on the combustion and emission characteristics of a methanol/diesel reactivity controlled compression ignition (RCCI) engine. Appl. Energy **106**, 184–197 (2013)
49. Lee, C.H., Wang, Y., Reitz, R.D.: CFD simulation of diesel sprays over a wide range of ambient gas densities using an improved gas jet spray model. Atomization and Sprays **21**(7), 591–609 (2011)
50. Kokjohn, S.L., Reitz, R.D.: Investigation of the roles of flame propagation, turbulent mixing, and volumetric heat release in conventional and low temperature diesel combustion. Journal of Engineering for Gas Turbines and Power **133**(10), 1–10 (2011)
51. Abani, N., Reitz, R.D.: Unsteady turbulent round jets and vortex motion. Phys. Fluids (1994-present) **19**(12), 125–102 (2007)
52. Ren, Z., Liu, Y., Lu, T., Lu, L., Oluwole, O.O., Goldin, G.M.: The use of dynamic adaptive chemistry and tabulation in reactive flow simulations. Combustion and Flame **161**(1), 127–137 (2014)
53. Tosatto, L., Bennett, B., Smooke, M.: A transport-flux-based directed relation graph method for the spatially inhomogeneous instantaneous reduction of chemical kinetic mechanisms. Combustion and Flame **158**(5), 820–835 (2011)
54. Hori, T., Senda, J., Kuge, T., Fujimoto, H.G.: Large eddy simulation of non-evaporative and evaporative diesel spray in constant volume vessel by use of KIVALES. Measurement **1**, 3337 (2006)
55. Zhou, L., Xie, M., Luo, K.H., Jia, M., Zhou, Q., Liu, H.: SAE Technical Paper (2013)
56. Lu, L., Lantz, S.R., Ren, Z., Pope, S.B.: Computationally efficient implementation of combustion chemistry in parallel PDF calculations. J. Comput. Phys. **228**(15), 5490–5525 (2009)
57. Zhou, L., Xie, M.-Z., Jia, M., Shi, J.-R.: Large eddy simulation of fuel injection and mixing process in a diesel engine. Acta Mechanica Sinica **27**(4), 519–530 (2011)